Chinese Chemical Letters 35 (2024) 108607

Contents lists available at ScienceDirect

Chinese Chemical Letters

journal homepage: www.elsevier.com/locate/cclet

Highly efficient photocatalytic conversion of CO_2 into CH_4 over Cu single atom promoted heterojunction: The effect of uplifted d-band center

Hao Zhang, Qian Liu, Zhurui Shen*

School of Materials Science and Engineering, Nankai University, Tianjin 300350, China

ARTICLE INFO

Article history:
Received 20 March 2023
Revised 21 April 2023
Accepted 24 May 2023
Available online 25 May 2023

Keywords:
Cu single atom
Heterojunction
CO_2 photoreduction
d-band center
DFT

ABSTRACT

Photoreduction of CO_2 to solar fuels has caused great interest, but suffers from low catalytic efficiency and poor selectivity. Herein, we designed a S-scheme heterojunction (Cu-TiO_2/WO_3) with Cu single atom to significantly boost the photoreduction of CO_2. Notably, the developed Cu-TiO_2/WO_3 achieved the solar-driven conversion of CO_2 to CH_4 with an evolution rate of 98.69 μmol g^{-1} h^{-1}, and the electron selectivity of CH_4 reached 88.5%. The yield was much higher than those of pristine WO_3, TiO_2/WO_3 and Cu-TiO_2 samples. Experimental and theoretical analysis suggested that the S-scheme heterojunction accelerated charge migration and inhibited the recombination of electron-hole pairs. Importantly, the charge separation effect of the heterojunction meliorated the position of the d-band. The uplifted d-band centers of Cu and Ti on Cu-TiO_2/WO_3 not only improved the electron interaction between Cu single atoms and substrate-TiO_2, accelerated the adsorption and activation of CO_2 on the active sites of Cu single atom, but also optimized the Gibbs free energies of CH_4 formation pathway, leading to excellent selectivity toward CH_4. This work provides new insights into the design of photocatalyst systems with high photocatalytic performance.

Excessive emissions of carbon dioxide (CO_2) caused by the ever-increasing consumption of fossil fuels have resulted in many environmental problems [1–8]. The conversion of photocatalytic CO_2 into value-added chemical products (CH_4, CO, C_2H_4, *etc.*) has attracted significant interest because it can utilize solar light and H_2O, that are abundant in nature, as energy and proton sources, respectively, without secondary pollution to the air environment. It is acknowledged that the prerequisite of improving the reduction performance of CO_2 photocatalysis is the establishment of suitable and high-performance photocatalysts. TiO_2 is one of the most widely utilized semiconductor materials in catalytic reactions owing to its environmental benignity, cost-effectiveness, and high physical and chemical stability [1,5,6,9]. More importantly, the conduction band (CB) of TiO_2 is relatively negative, which would improve the reduction ability of photogenerated electrons. However, the limited charge separation efficiency and optical absorption hinder the reduction performance of the CO_2 photocatalysis *via* TiO_2.

In the strategies of regulating activity of CO_2 photoreduction, constructing heterojunction with suitable semiconductors, photocatalysts with excellent performance can be obtained, which would facilitate charge separation by trapping photoelectrons [1,2,10–14]. Tungsten oxide (WO_3), has attracted much attention with relatively small bandgap (2.2–2.6 eV), low in toxicity as well as stable in acidic and oxidative conditions [10,14]. Importantly, WO_3 has the characteristic of band matching with TiO_2 [11,13], coupling the two semiconductors to build a heterojunction, which improves the charge separation by trapping the photoelectrons and extending the energy range of photoexcitation toward the visible range, seems to be an efficient strategy to promote the performance of CO_2 photoreduction. Generally, various heterostructures have been studied for photoreduction of CO_2 [1,10–14]. However, compare with conventional fuel production technologies, the efficiency of solar to fuel conversion is still very moderate. Thus, advanced strategies are required to design and fabricate a challenging heterojunction photocatalyst to improve efficiency of CO_2 conversion.

Metal co-catalysts have also been widely applied in many photochemical reactions because of their high activity and selectivity [15–24]. In particular, when tuned to the atomic scale, metal catalysts can maximize atomic utilization and accelerate the surface catalytic process; therefore, a number of atomically dispersed metals on semiconductors have emerged as effective platforms

* Corresponding author.
E-mail address: shenzhurui@nankai.edu.cn (Z. Shen).

https://doi.org/10.1016/j.cclet.2023.108607
1001-8417/

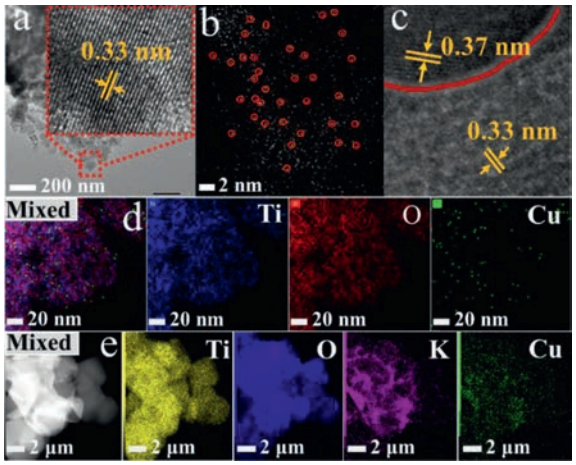

Fig. 1. Images of (HR)TEM over TiO_2 (a), AC HAADF-STEM over Cu-TiO_2 (b), HRTEM over Cu-TiO_2/WO_3 (c). EDX elemental mapping over Cu-TiO_2 (d) and Cu-TiO_2/WO_3 (e).

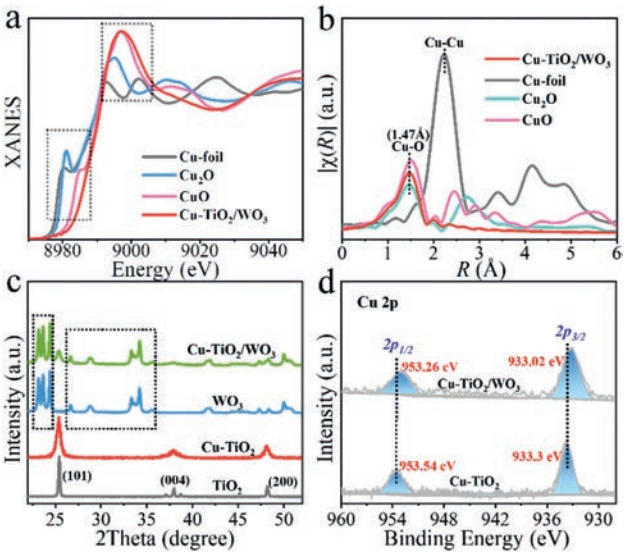

Fig. 2. Cu K-edge XANES (a) and Fourier transform of k^3-weighted Cu K-edge EXAFS (b) of Cu-TiO_2/WO_3 and the reference Cu foil, Cu_2O, and CuO. XRD patterns (c) of samples and Cu 2p of XPS (d) over Cu-TiO_2/WO_3.

for establishing high-performance photocatalysts in recent years [4,6,8,19]. Compared with noble metals (Au, Rh, and Pt), the earth-abundant metal Cu is regarded as one of the most attractive metal co-catalysts for producing hydrocarbons from CO_2 due to the diversity of reduction products [4,8,20–22]. For example, Li *et al.* [4] developed a photoinduction strategy to achieve the formation of Cu single atoms (SA) on a UiO-66-NH_2 support. Notably, the introduction of Cu SAs not only significantly enhanced transfer and separation efficiency, but also acted as active centers to facilitate the conversion of CO_2 to CHO* and CO* intermediates, leading to excellent selectivity toward methanol and ethanol. Likewise, wang *et al.* [7] designed single-atom Cu modified polymeric carbon nitride (CN), in which the C-Cu-N_2 single-atom catalytic site activated CO_2 molecules and reduced the energy barrier toward photocatalytic CO_2 reduction, resulting simultaneous production of CO, CH_4 and CH_3OH. Inspired by these efforts, the improvement of CO_2 reduction activity on heterojunction could be achieved *via* loading Cu SA on its surface. In fact, there are several reports concerning single atomic multi-heterojunctions on photoreduction of CO_2. However, the mechanism of CO_2 conversion is not well elaborated, especially the effect of charge separation on the d-band of metal single atom. It is known that the interaction between metal d-band and CO_2 molecular orbitals is directly reflected in the adsorption energy, the position of d-band center also determined by the interact with CO_2 molecular orbitals of intermediates in catalytic behavior of photocatalyst [25–28]. Therefore, the d-band center has proven to be an extremely useful electronic descriptor to explain photocatalytic CO_2 reduction selectivity.

Hence, in this work, Cu-TiO_2/WO_3 heterojunction was synthesized by a simple chemisorption strategy to investigate the activity and selectivity of CO_2 photocatalytic reaction. In the process, Cu single atoms were firstly loaded on the surface of TiO_2 (Cu-TiO_2) *via* reduction method, and then coupled with WO_3 to synthesize a S-scheme heterojunction photocatalyst to ensure efficient electron utilization and chemical transformation. Under simulated solar light irradiation, the Cu-TiO_2/WO_3 photocatalyst displayed an obviously enhanced photoreduction activity and selectivity toward CH_4. Using first-principles density functional theory (DFT) calculations, we revealed the decisive influence of charge separation effect of heterojunction on interaction between Cu single atom and TiO_2 substrate, and the d-band position.

The morphologies and microstructures of as-prepared samples were shown in Fig. 1 and Fig. S1 (Supporting information). In the high-resolution transmission electron microscope (HRTEM) images (Fig. 1a), bare TiO_2 was uniform and the lattice fringes of 0.33 nm correspond to the (101) planes of anatase-TiO_2 [1,6]. And in the aberration-corrected high-angle annular dark-field scanning transmission microscopy (AC HAADF-STEM) images, isolated bright spots were observed on Cu-TiO_2 sample, which indicated that Cu were homogeneously diffused on the surface of TiO_2 nanoparticles in the form of atoms rather than clusters. After Cu-TiO_2 was contacted with WO_3, a clear boundary line (red) was observed (Fig. 1c), and the lattice fringes with distances of 0.33 nm and 0.37 nm were attributed to the (101) crystal plane of TiO_2 and (200) crystal plane of WO_3, respectively [1,6]. The result indicated that the Cu-TiO_2/WO_3 heterojunction was successfully obtained. Thereafter, according to the energy-dispersive X-ray (EDX) mapping shown in Figs. 1d and e, Cu-TiO_2/WO_3 displayed homogeneous distribution of Ti, O, Cu and W elements. Besides, according to the result of inductive coupled plasma emission spectra (ICP) shown in Table S1 (Supporting information), the loading amount of Cu single atom in Cu-TiO_2/WO_3 was just slightly loss, which may be caused by cleaning during in the process of preparation.

To explore the coordination environment and chemical states of Cu atoms, X-ray absorption fine structure (XAFS) was measured on Cu-TiO_2/WO_3. As shown in Fig. 2a, the peak of Cu K-edge X-ray absorption near edge structure (XANES) located at 8997 eV of Cu-TiO_2/WO_3 was similar to that of CuO, indicating the existence of Cu single atom with a positive 2 valence. Subsequently, k^3-weighted Cu K-edge Fourier transform (FT) curve and wavelet transform (WT) analysis of Cu-TiO_2/WO_3 were shown in Fig. 2b and Fig. S2 (Supporting information), except for a main scattering peak at 1.47 Å attributed to the Cu-O coordination, the peak at 2.24 Å corresponding to Cu-Cu interaction in Cu-TiO_2/WO_3 was not detected, confirming the single atom dispersion of Cu. According to the fitting results of XANES shown in Table S2 (Supporting information), the Cu single atoms were coordinated with 4.0 ± 0.26 O atoms of TiO_2 with an average bond length of 1.922 ± 0.006 Å, which was slight shorter than Ti-O bond (1.94 Å) due to the lattice distortion and/or contraction in Cu-TiO_2/WO_3. Consequently, the tetrahedral oxygen-coordinated Cu-O_4 sites were anchored at the Ti sites, schematically shown in Fig. S3 (Supporting information).

Fig. 2c displayed the X-ray diffraction (XRD) patterns of samples. The spectra of TiO_2 agreed with simulated anatase struc-

ture (JCPDS No. 21–1272), and the introduction of Cu SA did not change TiO_2 crystallinity. For Cu-TiO_2/WO_3 heterojunction, besides the peaks of TiO_2, the peaks assigned to WO_3 (yellow line) were observed [1,14], indicating the successful construction of heterojunction. Next, as shown in Fig. S4a (Supporting information), X-ray photoelectron spectrum (XPS) of Cu-TiO_2/WO_3 verified the existence of Ti, O, Cu, and W. In Fig. S4b (Supporting information), the Ti 2p spectra of TiO_2 exhibited Ti $2p_{1/2}$ and Ti $2p_{3/2}$, respectively. A positive (0.21 eV) shift was observed in Cu-TiO_2, indicating a decreasing of electron density on Ti owing to the electron enrichment of Cu sites. For Cu-TiO_2/WO_3, a larger shift was happened (0.45 eV), suggesting that more electrons on Ti were transferred to Cu sites in the heterojunction. In Fig. 2d, the spectra of Cu 2p was divided into $2p_{1/2}$ and $2p_{3/2}$ on Cu-TiO_2 [8,21], respectively. While, the both peaks shifted to the lower binding energies (0.28 eV) in Cu-TiO_2/WO_3, indicating the electron density of Cu sites was increased. A similar tendency with Ti 2p appeared in W 3d XPS shown in Fig. S4c (Supporting information), which indicated that the electrons of W site of heterojunction also decreased. The results suggested that Cu-TiO_2/WO_3 heterojunction accelerated the charge migration behavior.

Ultraviolet-visible diffuse reflectance spectroscopy (UV–vis DRS) was applied to survey the optical property of samples. In Fig. S5a (Supporting information), comparing with Cu-TiO_2, the range of optical absorption over Cu-TiO_2/WO_3 further broaden due to the visible adsorption of WO_3, which was beneficial to CO_2 photoreduction. To reveal band structure of the heterojunction, the bandgap and Mott-Schottky plots were conducted and shown in Figs. S5b-e and Table S3 (Supporting information). According to the results, the valence bands (VB) of TiO_2 and WO_3 were 2.44, and 2.53 V, their conduct bands (CB) were −0.61 and 0.02 V [11,13], respectively. The movement of electrons in heterojunction photocatalyst can be described by the work functions (W) of semiconductors. W of TiO_2 and WO_3 were 4.69 and 5.05 eV [11,13]. When Cu-TiO_2/WO_3 heterojunction was formed, the free electrons would transfer from TiO_2 to WO_3 easily until the Fermi levels (Ef) tend to equilibrate at the interface. Concurrently, an internal electric field (IEF) was formed. When the heterojunction was exposed to light, photoelectrons were excited and transferred from VB to CB of WO_3 and TiO_2, respectively. Under the effect of IEF, the photoelectrons on CB of WO_3 easily migrated and combined with the holes on VB of TiO_2. This charge transfer behavior of Cu-TiO_2/WO_3 heterojunction was matched with the S-scheme mechanism [11,13], which was consistent with the XPS results. The illustration of charge transfer under simulated sunlight for efficient photocatalysis over Cu-TiO_2/WO_3 was shown in Fig. S6 (Supporting information). In this regard, efficient charge separation would be achieved. Finally, more photoinduced electrons would participate in the photocatalysis process. Comparing with E_0 (CO_2/CH_4 = −0.17 V *vs.* NHE, pH 0), Cu-TiO_2/WO_3 has the ability of photocatalytic reduction of CO_2 to CH_4.

To evaluate photocatalytic property of Cu-TiO_2/WO_3, CO_2 photoreduction experiment was performed under simulated sunlight irradiation with water as hole sacrificial reagents. To optimize the photoreduction performance, TiO_2 loaded with different amounts of Cu single atom and the heterojunction with different mass ratios of Cu-TiO_2 and WO_3 were also prepared. CO_2 photoreduction experiments of all samples were shown in Fig. 3a and Fig. S7 (Supporting information), both of pure TiO_2 and WO_3 converted CO_2 into CO, with formation rates of 3.28 and 1.08 μmol g^{-1} h^{-1}, respectively. After Cu SA introduced, CH_4 become the main product of CO_2 photoreduction, and a small amount of CO and C_2H_4 were also observed. Moreover, comparing to 0.5 and 2.0 mL, 1.0 mL of Cu^{2+} solution was the optimal volume and Cu-TiO_2 exhibited the supreme photocatalytic performance with formation rates of 32.29 μmol g^{-1} h^{-1} for CH_4. The results suggested that the Cu single

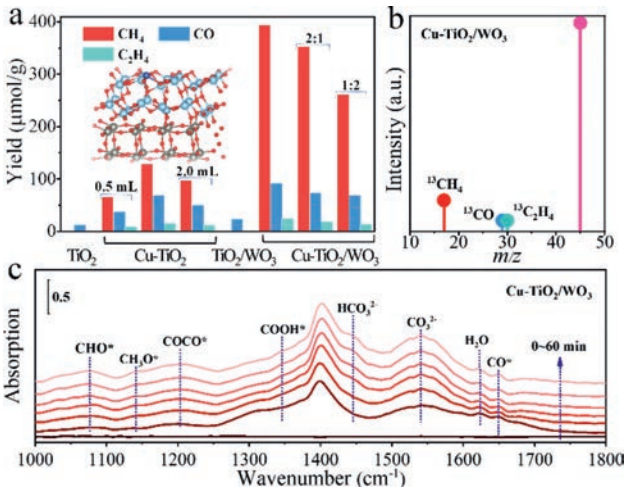

Fig. 3. Products from CO_2 photoreduction reaction (a), labeling test of $^{13}CO_2$ on Cu-TiO_2/WO_3 (b), *in-situ* FTIR spectroscopy measurement over Cu-TiO_2/WO_3 (c).

atom center may be a highly active site for CO_2 to CH_4. In addition, too small amount of Cu single atom would lead to insufficient active sites for photoreduction, and excessive ones would result in aggregation, which also affected the activity of CO_2 photoreduction. For Cu-TiO_2/WO_3 photocatalyst, it found that CH_4 was still the main product in CO_2 conversion. And the evolution rate of CH_4 reached 98.69 μmol g^{-1} h^{-1}, which was much higher than those of pristine WO_3, TiO_2/WO_3 and Cu-TiO_2 samples. The results indicated that the formation rate of CH_4 were significantly improved due to the charge separation effect of Cu-TiO_2/WO_3 heterojunction.

To further verify the role played by Cu single atom and the effect of charge migration on Cu-TiO_2/WO_3 heterojunction, TiO_2/WO_3 sample was prepared in the absence of Cu single atom. In Fig. 3a, it found that TiO_2/WO_3 only could convert CO_2 into CO, with a rate of 6.13 μmol g^{-1} h^{-1}, and no CH_4 was detected, suggesting that Cu site may be the key active center for the conversion of CO_2 to CH_4 on Cu-TiO_2/WO_3. Next, Cu-TiO_2 and WO_3 were mixed by simple mechanical stirring without interfacial chemical contact. This sample was named as Cu-TiO_2+WO_3 and its photoreduction result displayed in Fig. S7b (Supporting information) was just close to that of Cu-TiO_2, far lower than that of Cu-TiO_2/WO_3, indicating that the construction of Cu-TiO_2/WO_3 significantly improved the activity of Cu active sites due to the charge migration and separation, thereby accelerating the conversion of CO_2 to CH_4. In Table S4 (Supporting information), the selectivity of CH_4 was also calculated. For Cu-TiO_2/WO_3, the electron selectivity toward CH_4 was reached 88.5%, which were 15.1% higher than that of Cu-TiO_2, indicating that the charge separation effect of the heterojunction promoted the pathway reaction of CO_2 to CH_4. The above results indicated that the construction of Cu-TiO_2/WO_3 photocatalyst not only enhanced the activity of CO_2 photoreduction, but also increased the selectivity toward CH_4.

To further confirm the photoreduction of CO_2, ^{13}C isotope labeling and blank control tests were performed. As shown in Fig. 3b, the overwhelming peaks of m/z = 17 ($^{13}CH_4$), 29 (^{29}CO) and 30 ($^{13}C_2H_4$) rooted in $^{13}CO_2$ sources indicated that all reduction products were originated from the $^{13}CO_2$ rather than other carbonaceous impurities. Blank control experiments were shown in Fig. S8 (Supporting information), where no reduction product was detected in N_2 or in the absence of photocatalysts, light irradiation, and H_2O, indicating that CO_2 gas, photocatalyst, light irradiation, and H_2O were the prerequisites for the photoreduction of CO_2. Subsequently, the stability of the heterojunction was investigated. As shown in Fig. S9 (Supporting information), the XRD structure of

Cu-TiO_2/WO_3 did not change before and after photoreduction reaction. The result proved that Cu-TiO_2/WO_3 has a relatively stable structure.

Next, we studied charge-transfer properties to investigate the reason of the enhanced photocatalytic activity on Cu-TiO_2/WO_3. In Fig. S10a (Supporting information), the transient photocurrent of heterojunction was enhanced significantly compared with those of other samples, implying that more effective charge separation over Cu-TiO_2/WO_3. And in Fig. S10b (Supporting information) Cu-TiO_2/WO_3 showed a marginally lowest PL signal, indicating more effective retardation of the charge recombination [14]. Electrochemical impedance spectroscopy (EIS) can also reflects the charge-transfer behavior. As shown in Fig. S10c (Supporting information), Cu-TiO_2/WO_3 has the lowest charge-transfer resistance of all samples, suggesting that more efficient transmission of charge have been achieved in Cu-TiO_2/WO_3. According to the results, it demonstrated that the S-scheme heterojunction could promote the migration and separation of surface photogenerated charges, thus improving photocatalytic performance of CO_2, which provided a clear evidence for electron transfer within several components of Cu-TiO_2/WO_3. Time-resolved photoluminescence (TRPL) profiles of samples were measured to further reveal the efficient separation of photogenerated carriers. At the excitation wavelengths (E_W) of 425 nm, the fitted decay curves disclose the lifetime (τ) and percentage (Rel.%) of charge carriers. As shown in Fig. S10d and Table S5 (Supporting information), Cu-TiO_2/WO_3 has a lowest percentage of τ1-carriers than other samples, indicating that the charge recombination was further inhibited due to the charge migration [14]. The average carrier lifetime of Cu-TiO_2/WO_3 (τ_a = 8.86 ns) was higher than that Cu-TiO_2 (4.92 ns), which was attributed to efficient transfer and separation of charges over Cu-TiO_2/WO_3 heterojunction. Therefore, it was not surprising that the Cu-TiO_2/WO_3 composite sample exhibit improved photocatalytic CO_2 reduction performance.

To understand the reaction mechanism of CO_2 photoreduction over Cu-TiO_2/WO_3, *in situ* FTIR measurements were performed to investigate the intermediates in the process of CO_2 conversion. As shown in Fig. 3c, the peaks located at 1075, 1145 and 1341 cm^{-1} were detected and ascribed to the CHO*, CH_3O*, and COOH* intermediates [29–32], respectively, which were the crucial groups for CO_2 conversion to CH_4. A new peak at 1203 cm^{-1} was observed and ascribed to COCO* group [33], a crucial C-C coupling intermediate of C_2H_4 formation. Additionally, the peak at 1659 cm^{-1} corresponded to the C=O stretching belonging to the CO* intermediate [34]. The *in situ* FTIR was agreed well with the results of CO_2 photoreduction test on Cu-TiO_2/WO_3. Based on the results, it speculated that Cu sites converted the adsorbed CO_2 to COOH*, CO*, CHO* and CH_3O* intermediates with the participation of protons and electrons, which in turn to produce CH_4. For weaker adsorbed groups [34], such as CO*, could be desorbed from the Cu active sites to generate CO gas. Meanwhile, partial CO* would also couple with the neighbor CO* to form COCO* intermediates, and finally form C_2H_4 with the assistance of multiple electrons and protons.

Next, DFT calculation was applied to examined the mechanism of CO_2 photoreduction on Cu-TiO_2/WO_3 photocatalyst. The model structure of the heterojunction was built by TiO_2 (101) and WO_3 (200) planes by replacing the Ti with Cu atoms. To further confirm the active site of the heterojunction, the adsorption energies of CO_2 on different metal sites were calculated and shown in Table S6 (Supporting information). According to the results, it proved that the Cu single atom site was the optimal active center in Cu-TiO_2 and Cu-TiO_2/WO_3 photocatalysts for CO_2 to CH_4. Next, Gibbs free energies (ΔG) were calculated in the premise of Cu single atom as active site, and shown in Figs. 4a and b and Table S7 (Supporting information). The ΔG of photoreduction of CO_2 to COOH*, CO*, CHO*, CH_3O* and CH_4 formation were displayed in Fig. 4a.

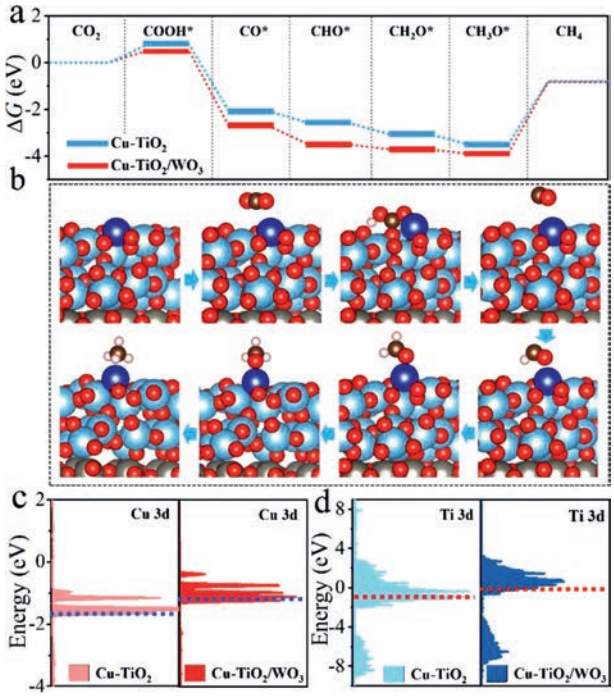

Fig. 4. Free-energy diagrams of CO_2 photoreduction over Cu-TiO_2 and Cu-TiO_2/WO_3 calculated from DFT (a), structure models of CO_2 to CH_4 pathway over Cu-TiO_2/WO_3 (b), the partial density of states (PDOS) of Cu-TiO_2 (c) and Cu-TiO_2/WO_3 (d) and the dashed lines represent the positions of d-band centers.

Along with the hydrogen proton (H^+) produced by water hydrolysis, the C bond of CO_2* was interacted with a pair of proton and electron to form COOH*. According to the calculated results, it found that the whole process of CO_2-to-CH_4 conversion on the Cu-TiO_2/WO_3 was more favorable in thermodynamics behavior than that on the Cu-TiO_2 surface. And the formation of COOH* intermediate was the rate-limiting step for both photocatalysts. For Cu-TiO_2/WO_3, an energy of 0.54 eV was needed to complete the step of CO_2 → COOH*. By contrast, ΔG of 0.79 eV (ΔG_{COOH^*} - ΔG_{CO_2}) was essential in endothermic reaction of Cu-TiO_2, suggesting the structure of Cu-TiO_2/WO_3 could efficiently lower the formation energy of key COOH* intermediate. From the results, it suggested that more electrons were transferred to Cu active sites from TiO_2 due to the charge separation effect of the heterojunction, which helped to optimize the rate-limiting step and promote the conversion of CO_2-to-CH_4.

Typically, the adsorption and activation of CO_2 is also critical for photocatalytic reduction [29]. Thus, the molecule structure of CO_2 before and after adsorption on the catalyst surface was calculated. In Table S8 (Supporting information), comparing with Cu-TiO_2, the CO_2 adsorbed on Cu-TiO_2/WO_3 has a smaller C-O-C angle, and longer C=O bonds, resulting in more curved configuration of adsorbed CO_2 and easier cleavage of C=O bonds [35,36]. Furthermore, in Table S9 (Supporting information), the adsorption energy of CO_2 on heterojunction was lower than Cu-TiO_2, indicating CO_2 adsorption and activation were easier to occurred on its surface.

Electronic properties of the catalyst were further carried out and analyzed to figure out the underlying factors governing the significant activity of the heterojunction, Firstly, the feature of CO_2 adsorption was further evaluated through the partial density of states (PDOS) on Cu active site, and the results were shown in Fig. S11 (Supporting information). When the O atom of CO_2 molecule was adsorbed on the Cu-TiO_2/WO_3 surface, the peaks shifted to lower energy than that of Cu-TiO_2, suggesting that the orbital coupling of CO_2 molecule with Cu active site of Cu-TiO_2/WO_3 was

more prone to carry out [37]. Next, the d-band center of Cu site was further explored to elaborate the adsorption behavior. In Fig. 4c and Table S10 (Supporting information), it suggested that the d-band centers of Cu in two catalysts depended on its local coordination environment, and was calculated to be −1.49 (Cu-TiO_2/WO_3) and −1.77 eV (Cu-TiO_2). Further analysis found that a more remarkable overlap between Cu 3d in Cu-TiO_2/WO_3 and O 2p of CO_2 at the identical position. Apparently, more substantial orbital and electron interactions of Cu sites and O were present than that of Cu in Cu-TiO_2, which uplifted the d-band center of Cu-TiO_2/WO_3 closer to the Fermi level. Such changes in the d-band centers of Cu were precisely correlated with the adsorption energy of key COOH* intermediates. In addition, the d-band of Ti was also calculated to elaborate the electron interaction between the Cu SA and the substrate TiO_2 in the heterojunction. As shown in Fig. 4d, comparing with Cu-TiO_2, the d-band of Ti become narrowed in Cu-TiO_2/WO_3, and the center of the d-band was also uplifted and closer to the fermi level, indicating more stronger interaction between the Cu SA sites and TiO_2 substrate.

The S-scheme heterojunction of coupling TiO_2 supported single Cu atoms with WO_3 provided an efficient method for charge separation and migration. The results showed that Cu single atom played a key role as active centers in CO_2 photoreduction over Cu-TiO_2/WO_3 photocatalyst, and the heterojunction significantly improved the mobility efficiency of surface photogenerated charge based on the unique advantages of S-scheme. Moreover, the charge separation effect of the heterojunction further promoted the adsorption and activation of CO_2 on Cu active sites. Importantly, the uplifted d-band centers of Cu and Ti of Cu-TiO_2/WO_3 photocatalyst enhanced the electron interaction between Cu single atom and TiO_2 substrate, and optimized the Gibbs free energies of CH_4 formation. The specific pattern of combining single-atom and heterojunction fully exploits the highly efficient charge separation to open up a new channel for the design of efficient photocatalyst systems.

Declaration of competing interest

The authors declare that they have no known competing financial interests or personal relationships that could have appeared to influence the work reported in this paper.

Acknowledgments

This work was supported by the grants from the National Natural Science Foundation of China (Nos. 21872102 and 22172080) and the Tianjin "Project + Team" innovation team, 2020.

Supplementary materials

Supplementary material associated with this article can be found, in the online version, at doi:10.1016/j.cclet.2023.108607.

References

[1] F.Y. Xu, K. Meng, B. Cheng, et al., Nat. Commun. 11 (2020) 4613.
[2] T. Butburee, Z.X. Sun, A. Centeno, et al., Nano Energy 62 (2019) 426–433.
[3] S. Huang, H. Yi, L. Zhang, J. Hazard. Mater. 393 (2020) 122324.
[4] T. Wang, F.L. Sun, S.J. Liu, et al., Appl. Catal. B: Environ. 325 (2023) 122339.
[5] Y.Z. Zhang, B.Q. Xia, J.R. Ran, et al., Adv. Energy Mater. 10 (2020) 1903879.
[6] B.H. Lee, E. Gong, M. Kim, et al., Energy Environ. Sci. 15 (2022) 601–609.
[7] J. Wang, T. Heil, B. Zhu, et al., ACS Nano 14 (2020) 8584–8593.
[8] Y.Y. Yu, X.A. Dong, P. Chen, et al., ACS Nano 15 (2021) 14453–14464.
[9] X.Z. Qian, W.Y. Yang, S. Gao, et al., ACS Appl. Mater. Interfaces 12 (2020) 55982–55993.
[10] F. Duanmu, Z. Shen, Q. Liu, S. Zhong, H. Ji, Chin. Chem. Lett. 31 (2020) 1114–1118.
[11] Y. Sun, Y. Han, X. Song, et al., J. Photochem. Photobiol. B 233 (2022) 112480.
[12] Y.F. Jia, J.J. Li, Z.J. Liu, et al., Chem. Eng. J. 437 (2022) 135300.
[13] L.B. Wang, B. Cheng, L.Y. Zhang, J.G. Yu, Small 17 (2021) 2103447.
[14] H.H. Gong, Y.F. Zhang, Y. Cao, et al., Appl. Catal. B: Environ. 237 (2018) 309–317.
[15] X. Shi, L.N. Cao, M. Chen, Y. Huang, Chin. Chem. Lett. 33 (2022) 5023–5029.
[16] P.G. Liu, Z.X. Huang, X.P. Gao, et al., Adv. Mater. 34 (2022) 2200057.
[17] L. Jin, E. Shaaban, S. Bamonte, et al., ACS Appl. Mater. Interfaces 13 (2021) 38595–38603.
[18] S. Gong, F. Rao, W. Zhang, et al., Chin. Chem. Lett. 33 (2022) 4385–4388.
[19] J. Xiong, M. Zhang, M. Lu, et al., Chin. Chem. Lett. 33 (2022) 1313–1316.
[20] F. Chen, X.L. Wu, C.Y. Shi, et al., Adv. Funct. Mater. 31 (2021) 2007877.
[21] X.Y. Lu, S.S. Gao, H. Lin, et al., Adv. Mater. 32 (2020) 2002246.
[22] G. Wang, C.T. He, R. Huang, et al., J. Am. Chem. Soc. 142 (2020) 19339–19345.
[23] G. Wang, R. Huang, J.W. Zhang, et al., Adv. Mater. 33 (2021) 2105904.
[24] D.T. Chen, L.H. Zhang, J. Du, et al., Angew. Chem. Int. Ed. 60 (2021) 24022–24027.
[25] Y. Zhao, Z.D. Han, G.Y. Gao, et al., Adv. Funct. Mater. 31 (2021) 2104976.
[26] J. Fu, K. Jiang, X. Qiu, J. Yu, M. Liu, Mater. Today 32 (2020) 222.
[27] X. Cai, F. Wang, R. Wang, et al., J. Mater. Chem. A 8 (2020) 7350.
[28] M. Hammerschmidt, S. Döpking, S. Burger, S. Matera, J. Phys. Chem. C 124 (2020) 3177.
[29] X.L. Yang, S.Y. Wang, N. Yang, et al., Appl. Catal. B: Environ. 259 (2019) 118088.
[30] J.C. Zhu, W.W. Shao, X.D. Li, et al., J. Am. Chem. Soc. 143 (2021) 18233–18241.
[31] F. Huang, Y.C. Deng, Y.L. Chen, et al., Nat. Commun. 10 (2019) 4431.
[32] T. Cheng, A. Fortunelli, W.A. Goddard lii, Proc. Natl. Acad. Sci. U. S. A. 116 (2019) 7718–7722.
[33] J.W. Wang, L.Z. Qiao, H.D. Nie, et al., Nat. Commun. 12 (2021) 813.
[34] S. Barman, A. Singh, F.A. Rahimi, T.K. Maji, J. Am. Chem. Soc. 143 (2021) 16284–16292.
[35] G. Wang, Z. Chen, T. Wang, D. Wang, J. Mao, Angew. Chem. Int. Ed. 61 (2022) 202210789.
[36] R. Li, D. Wang, Nano Res. 15 (2022) 6888–6923.
[37] X. Sun, L. Sun, G. Li, et al., Angew. Chem. Int. Ed. 61 (2022) 202207677.